Quality by Design-Assisted Development of Crisaborole-Loaded Ethosomes for Enhanced Topical Delivery in Psoriasis

Sonam M Gandhi[1*], Ronak Dedania[2]

[1]Department of Pharmaceutics, S.S. Agrawal Institute of Pharmacy, Navsari-396445 India.

[2]Department of Pharmaceutics, Bhagwan Mahavir College of Pharmacy, Surat – 394110, India.

Corresponding Author

Sonam M Gandhi
S. S. Agrawal Institute of Pharmacy
Agrawal Road, Navsari – 396445,
Gujarat, India.
sonamgandhi48@gmail.com
Orcid id - 0009-0003-3586-9689

Abstract:

Crisaborole (CRS), a non-steroidal phosphodiesterase-4 inhibitor, is a promising topical agent for psoriasis, but its therapeutic efficacy is limited by its poor aqueous solubility and restricted skin permeation. The aim of the present study was to develop and optimise CRS-loaded ethosomes by Quality by Design (QbD) approach for enhanced topical delivery. Thin-film hydration method was employed to formulate ethosomes and Box–Behnken design was applied for optimisation to study the effect of cholesterol concentration, ethanol concentration and sonication time on vesicle size, polydispersity index (PDI) and entrapment efficiency. The optimised formulation had a vesicle size of 181.3 nm, 80% entrapment efficiency and PDI of 0.210, which were in close agreement with the model predicted values. Transmission electron microscopy revealed spherical vesicles uniformly distributed without aggregation. The optimised ethosomes exhibited 85% cumulative drug release over 12 h and release was best fitted to the Higuchi model (R 2 = 0.9867) indicating the diffusion controlled release kinetics. In the imiquimod induced psoriasis mouse model, the optimised ethosomal gel decreased PASI score from 4.00 to 1.00, ear thickness from 0.46 to 0.26 mm, spleen weight from 0.198 to 0.105 g and significantly suppressed the levels of IL-6 (70.33 to 58.67 pg/mg protein) and IL-22 (452.67 to 107.67 pg/mg protein) with concurrent histopathological improvement. The results indicate the potential of QbD-optimized CRS-loaded ethosomes as an effective nanovesicular platform for topical psoriasis therapy.

Keywords: Crisaborole; Ethosomes; Quality by Design; Psoriasis; Topical drug delivery.

Graphical abstract:

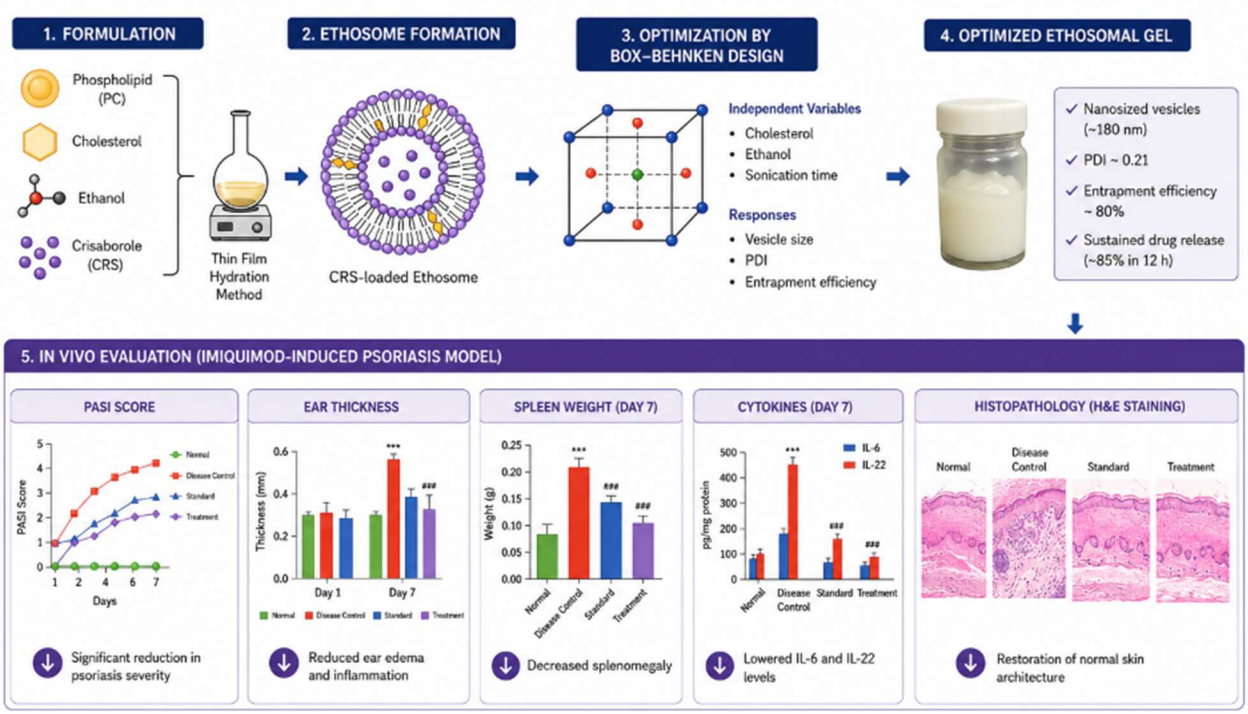

1.Introduction

Psoriasis is a chronic immune-mediated inflammatory dermatosis characterised by epidermal hyperproliferation, abnormal keratinocyte differentiation, and sustained activation of innate and adaptive immune pathways[1]. The disease affects approximately 2–3% of the world population and is associated with significant physical, psychosocial and economic burden[2]. The pathogenesis of psoriasis is a complicated interaction of genetic predisposition, environmental influences and immune dysregulation. The interleukin (IL)-23/IL-17 axis is the key player in the initiation and progression of the disease. The chronic inflammation is caused by the ongoing production of pro-inflammatory cytokines, including tumour necrosis factor-α (TNF-α), IL-17 and IL-23, resulting in the formation of the characteristic erythematous and scaly plaques[3].

Although topical corticosteroids, vitamin D analogues, retinoids, systemic immunosuppressants, and biologic therapies remain the cornerstone of psoriasis management, their long-term clinical utility is often restricted by local and systemic adverse effects, poor patient adherence, and the need for prolonged treatment[4]. Consequently, the development of safer and more effective therapeutic approaches capable of achieving targeted drug delivery while minimizing systemic exposure has become an important area of pharmaceutical research[5].

CRS is a boron-containing phosphodiesterase-4 (PDE4) inhibitor that exerts potent anti-inflammatory activity through intracellular modulation of cyclic adenosine monophosphate (cAMP) signaling pathways. Inhibition of PDE4 prevents cAMP degradation, resulting in downregulation of multiple pro-inflammatory cytokines implicated in psoriatic pathophysiology[5]. Owing to its non-steroidal mechanism of action and favorable safety profile, CRS has emerged as a promising therapeutic candidate for inflammatory skin disorders. However, the therapeutic efficacy of topically administered CRS remains constrained by the barrier properties of the stratum corneum, which significantly limit drug permeation, cutaneous retention, and bioavailability at the target site[6].

Nanovesicular drug delivery systems have gained considerable attention as advanced platforms for enhancing dermal and transdermal transport of therapeutic agents[7]. Among these systems, ethosomes represent a unique class of phospholipid-based vesicles containing relatively high concentrations of ethanol[8]. The synergistic interaction between phospholipids and ethanol imparts remarkable deformability and elasticity to the vesicular membrane, enabling efficient penetration

through the highly organized lipid architecture of the stratum corneum[9]. Furthermore, ethosomes offer several advantages, including enhanced drug encapsulation, improved skin permeation, prolonged drug retention, controlled release behavior, and superior biocompatibility[9].

Recent advances in nanocarrier-mediated topical therapy have demonstrated that ethosomal systems can significantly improve the dermal delivery of anti-inflammatory and poorly permeable therapeutic agents[10]. The nanoscale size and flexible vesicular structure facilitate deeper skin penetration and localized drug accumulation within inflamed tissues, thereby enhancing therapeutic performance. In addition, incorporation of ethosomal dispersions into hydrogel-based formulations may further improve formulation stability, skin residence time, and patient acceptability during chronic treatment[11].

Considering the anti-inflammatory potential of CRS and the exceptional skin-penetrating capabilities of ethosomal vesicles, the development of a CRS-loaded ethosomal delivery system represents a rational strategy for improving topical psoriasis therapy. Therefore, the present study was undertaken to formulate and optimize CRS-loaded ethosomes and to evaluate their physicochemical characteristics, skin permeation behavior, and therapeutic potential as an advanced nano vesicular platform for the management of psoriasis.

2. Materials and Methods

2.1 Materials

CRS was procured from MedChemExpress (MCE), India, and used as the active pharmaceutical ingredient. Phospholipid was obtained from Hi Media Laboratories Pvt. Ltd., Mumbai, India, which is helpful for the vesicle formation. Ethanol was purchased from Merck Life Science Pvt. Ltd., Mumbai, India, and used as the alcoholic phase for ethosome preparation. Propylene glycol was obtained from Central Drug House (CDH), New Delhi, India, and used as a co-solvent to improve drug solubility and formulation performance. For the preparation of the ethosomal gel, Carbopol 934 was procured from Taiwan Hon Chuan Enterprise Co. Ltd. through its authorized Indian distributor, and used as the gelling agent. Triethanolamine was purchased from Loba Chemie Pvt. Ltd., Mumbai, India, and added to adjust the pH to a suitable range for topical application.

2.2 Methodology

2.2.1 Preformulation Studies

Preformulation studies were carried out to assess the major physicochemical properties of the drug and excipients prior to formulation development. These studies offered the fundamental information for the design of a stable, effective and reproducible topical dosage form[12].

2.2.2 Organoleptic Characterization

Organoleptic characteristics of CRS were evaluated as a preliminary physicochemical evaluation before formulation development. The drug sample was visually examined for colour, appearance, texture and odour under normal laboratory conditions using clean glass Petri dishes (Borosil®, Borosil Ltd., Mumbai, India). The sample was manipulated with a stainless steel spatula and weighed accurately on an analytical balance (AUW220D, Shimadzu Corporation, Kyoto, Japan). These observations were documented in order to verify identity and quality attributes of the active pharmaceutical ingredient and to establish baseline characteristics relevant to formulation design[13].

2.2.3 Determination of Melting Point

Melting point of CRS was determined by capillary tube method using digital melting point apparatus (MPA100 Opti melt, Stanhope-Seta Ltd., Surrey, United Kingdom). A small amount of drug was weighed accurately on an analytical balance (AUW220D, Shimadzu Corporation, Kyoto, Japan) and carefully packed in a glass capillary tube sealed at one end. The capillary tube was placed in the melting point apparatus and heated at a controlled rate until the sample was completely melted. The melting temperature was taken and compared with the reported values for purity and crystalline nature of drug substance[14].

2.2.4 Differential Scanning Calorimetry

Thermal characterization and drug–excipient compatibility of CRS were evaluated using a Differential Scanning Calorimeter (DSC 60 Plus, Shimadzu Corporation, Kyoto, Japan). The analysis was carried out on the pure drug and a physical mixture of CRS, cholesterol, and ethanol (1:1:1) under a nitrogen atmosphere. Approximately 5 mg of each sample was accurately weighed, sealed in aluminum pans, and heated from 40°C to 300°C at a heating rate of 10°C/min with a nitrogen flow rate of 60 mL/min. The resulting thermograms were analyzed to identify the

characteristic melting endotherm of CRS and to detect any changes in thermal behavior. Variations in peak position, peak shape, or the appearance of additional thermal events were carefully assessed as indicators of possible interactions between the drug and formulation excipients. The absence of significant changes in the thermograms was considered evidence of thermal compatibility among the formulation components[15].

2.2.5 Solubility Analysis

Solubility characteristics of CRS were determined by solubility measurement in different solvents like distilled water, ethanol, acetone, chloroform, diethyl ether and phosphate buffer (pH 7.4) for selection of suitable formulation components. CRS in excess was separately added to 20 mL of each solvent in tightly closed borosilicate glass vials. The vials were intermittently shaken for 24 h at room temperature (25 ± 2°C) until equilibrium saturation was attained. At the end of the equilibration period, the samples were filtered through a 0.45 µm nylon membrane filter (Millipore, Merck KGaA, Darmstadt, Germany) to eliminate any undissolved drug particles. The filtrates were appropriately diluted with respective solvent and analysed by UV-Visible spectrophotometer (UV-1900i, Shimadzu Corporation, Kyoto, Japan) at wavelength of 296 nm. The solubility of CRS in each solvent system was determined from the respective calibration curve and expressed in mg/mL[16, 17].

2.2.6 Identification of CRS and Drug–Excipient Compatibility Study by FTIR

Fourier Transform Infrared (FTIR) spectroscopy was used to examine the identification of CRS and its compatibility with the chosen formulation excipients. An FTIR spectrophotometer (Cary 630 FTIR, Agilent Technologies, Santa Clara, California, USA) was used to conduct the analysis. At a spectral resolution of 4 cm, infrared spectra were captured within the wavenumber range of 4000–500 cm^{-1}[18]. The drug's validity and structural integrity were verified by comparing the distinctive absorption peaks found for CRS with the published reference spectra. A physical mixture of CRS, cholesterol, and Span 80 in a 1:1:1 ratio was created in order to assess possible interactions between the medication and excipients. For a duration of 14 days, the pure medication and the physical mixture were placed in amber-colored glass vials that were tightly sealed and kept at 40 ± 2°C and 75 ± 5% relative humidity. These settings were chosen to mimic potential stress-related alterations that can take place during the production and storage of formulations. The stored samples' FTIR spectra were obtained using the same equipment after the incubation time. To find any alterations

in the distinctive functional group vibrations, the spectra of the stressed physical combination and the pure drug were closely compared. Because these data could point to potential physicochemical interactions between CRS and the excipients, special attention was paid to changes in peak locations, alterations in peak intensity, disappearance of typical bands, or the formation of novel absorption peaks. The medicine and the chosen formulation components were thought to be satisfactorily compatible if there were no noticeable spectral alterations[19, 20].

3. Preparation of CRS loaded ethosomes

The thin-film hydration method was used to create ethosomes loaded with CRS. In a round-bottom flask, CRS and phospholipid were first dissolved in a chloroform:methanol solvent system (2:1, v/v). A thin lipid layer formed along the flask's inner surface after the organic solvents were extracted under low pressure using a rotary evaporator (RV 8, IKA, Staufen, Germany). In order to encourage vesicular formation, the dried lipid film was then hydrated with phosphate-buffered saline (PBS, pH 7.4) containing ethanol while being continuously stirred for 45 minutes. A probe Sonicator (Sonics Vibra-Cell, Sonics & Materials Inc., Newtown, USA) operating at 20% amplitude with alternating pulse cycles of 10s on and 10s off for a total of 8 minutes was used to further process the obtained dispersion. This stage made it easier to produce nanoscale vesicles with better homogeneity. The completed ethosomal suspension was gathered and kept at 4 ± 2 °C till additional formulation and physicochemical analysis was conducted[21].

3.1 Experimental Study Design

Using Box-Behnken Design (BBD) produced by Design-Expert® software (Version 13, Stat-Ease Inc., Minneapolis, MN, USA), an optimisation strategy based on Quality by Design (QbD) was implemented. The design was used to methodically examine how important formulation factors affected the physicochemical properties of ethosomes loaded with CRS. Based on initial research, three independent formulation factors were chosen: sonication time (X_3), ethanol concentration (X_2), and phospholipid content (X_1). Three levels of evaluation were used for each factor: -1, 0, and +1. These factors were evaluated as dependent responses on vesicle size (Y_1), entrapment efficiency (Y_2), and polydispersity index (Y_3). The Box-Behnken statistical model produced 13 experimental runs in all. Analysis of variance (ANOVA) was applied to the collected data in order to assess the importance of each individual element as well as the effects of their interactions. To determine the link between measured responses and independent factors, contour plots, polynomial equations,

and three-dimensional response surface plots were created. In order to maximise entrapment efficiency while minimising vesicle size and polydispersity index, the optimal formulation was chosen using the desirability function[22]. **Table 1** represent the independent and dependent variables used in BBD for CRS loaded ethosomes. **Table:2** represent the BBD experimental runs for optimization of CRS loaded ethosomes formulation

Table:1 Independent and dependent variables used in BBD for CRS loaded ethosomes

Independent Variable	Code	Low (-1)	Medium (0)	High (+1)
Phospholipid (% w/v)	**X_1**	1	2	3
Ethanol (% v/v)	**X_2**	20	30	40
Sonication time (Minute)	**X_3**	5	10	15
Dependent variables (responses) Target				
Vesicle Size (nm)	**Y_1**	Minimize		
Entrapment Efficiency (%)	**Y_2**	Maximize		
Polydispersity Index (PDI)	**Y_3**	Minimize		

Table:2 BBD experimental runs for optimization of ethosomes formulation

Run	A: Cholesterol (mg)	B: Ethanol (%)	C: Sonication Time (min)	Response 1: Vesicle Size (nm)	Response 2: Entrapment Efficiency (%)	Response 3: PDI
1	3	40	10	219.6	88.87	0.28
2	3	20	10	245.8	83.65	0.22
3	1	30	5	161.7	68.43	0.18
4	3	30	5	237.8	84.42	0.25
5	2	40	15	132.9	73.88	0.30
6	1	20	10	185.2	68.93	0.16

7	2	20	5	187.8	70.12	0.20
8	2	40	5	140.3	72.18	0.27
9	1	40	10	130.8	67.92	0.24
10	1	30	15	149.7	65.46	0.21
11	2	30	10	171.6	74.82	0.19
12	2	20	15	193.4	71.08	0.23
13	3	30	15	212.6	85.48	0.29

3.2 Characterization of APT-loaded niosomes

3.2.1 Particle size, polydispersity index (PDI) and zeta potential determination

A Zetasizer Nano ZS90 (Malvern Instruments, Malvern, Worcestershire, United Kingdom) was used to measure vesicle size, PDI, and zeta potential using electrophoretic mobility and DLS. Test samples were diluted 1:500 (v/v) with deionised water for measuring purposes[23].

3.2.2 Surface Morphology Analysis by Transmission Electron Microscopy (TEM)

A Tecnai transmission electron microscope with an accelerating voltage of 50 kV, provided by FEI Company, Eindhoven, The Netherlands, was used to analyse the surface morphology of niosomes. TEM (Tecnai, Eindhoven, Netherlands) was used to analyse the surface morphology of CRS-loaded ethosomes. After mounting the sample on a copper grid coated with carbon, it was diluted with deionised water and allowed to air dry. After that, the sample was examined under a microscope at room temperature using a 50 kV accelerating voltage[24].

3.2.3 Entrapment efficiency (EE) measurement

The entrapment effectiveness of APT in niosomes was estimated using the ultracentrifugation method (31). To extract the free drug from the niosomes, an ultracentrifugation was performed at 17,000 rpm (≈28,000 x g, Rotor Radius 10.2 cm) for 90 minutes at 4°C. The UV-Visible spectrophotometer (UV-1800), manufactured by Shimadzu in Kyoto, Japan, was used to quantitatively estimate APT during entrapment efficiency and in vitro drug release investigations at a wavelength of 340 nm (32). No excipient interference was seen in blank formulations, and a calibration graph (2–20 µg/mL) was generated at 340 nm with r^2=0.999(28). By deducting the free drug content from the total drug content, the entrapment efficiency of the drug is evaluated, and the entrapment efficiency (%) is computed using the formula (33).

% Entrapment efficiency = (Entrapped drug) / (Total drug) x100

3.2.4 *In vitro* drug release study

The dialysis bag method was used to measure the in vitro release of CRS from the ethosomes with a molecular weight cut-off value of 12–14 k Da. The results were compared with a solution of the pure medication (34). A cellulose dialysis bag that had already been soaked was filled with a volume of ethosome suspension equal to 5 mg of the medication. After that, it was submerged in 100 millilitres of pH 7.4 PBS buffer solution, kept at 37±1°C, and constantly agitated at 100 rpm. 2 mL samples of the medium were taken throughout a 12-hour period at prearranged intervals and replaced with new buffer solution. The specific absorbance of CRS at 340 nm was measured using a UV spectrophotometer to quantify the concentration of CRS in each sample. Higuchi, Korsmeyer-Peppas, zero-order, and first-order equations were fitted to the optimized formulation's release profile using linear regression analysis. For more investigation, the model with the highest correlation coefficient was chosen[25].

3.2.5 Physical Stability of APT-Loaded ethosomes

Stability experiments were conducted on the optimised APT niosomal formulation to track changes in vesicle properties and potential drug leakage during storage. For ninety days, freshly made niosomal dispersion was refrigerated at 4 °C in sealed glass vials. To evaluate any changes in structural integrity over time, samples were taken out at predefined intervals (30 and 90 days) and examined for particle size, entrapment efficiency, and PDI[26].

3.3 Formulation of CRS Ethosomal Gel

To achieve complete gel formation, a 1% w/w solution of Carbopol 934 was dispersed in an aqueous medium and allowed to hydrate for 12 h. Subsequently, triethanolamine at a concentration of 0.1% w/w was added to neutralize the dispersion and obtain a translucent gel. The optimized ethosomal dispersion containing CRS (as obtained from optimization studies) was then incorporated into the Carbopol gel base to achieve a final drug concentration of 0.25% w/w. Furthermore, benzalkonium chloride at a concentration of 0.01% w/w was incorporated into the formulation as a preservative[27].

3.4 Characterization of CRS Loaded Ethosomal Gel

The visually inspected properties of the CRS-loaded ethosomal gel included the color, homogeneity, consistency, and any phase separation, aggregation, or particulates that might be present, which was

further supported by gentle finger rub. The pH value of the prepared gel formulation was assessed using a calibrated digital pH meter by inserting an electrode in the sample (41). The rheological behavior of the ethosomal gel was measured using a Brookfield LV viscometer (spindle T-C) (Brookfield Engineering Laboratories, Middleboro, Massachusetts, USA). The spreadability of the CRS-loaded ethosomal gel was measured by slide-over-slide method proposed by Asghar Z et al.and his team (2023)[28]. In this process, a fixed amount of gel (0.5 g) was placed evenly on the glass slide and another glass slide was placed over it. After placing a string on the pan and applying a certain weight on the pan, the time taken by the upper slide to slide through a certain distance was recorded. The coefficient of spreadability (S) is calculated by using the following formula[29]:

$$\mathbf{S = \frac{MXL}{T}}$$

Where:

S = Spreadability coefficient (g·cm/s)

M = Weight tied to the upper slide (g)

L = Length moved by the glass slide (cm)

T = Time taken (s)

3.5 *In vivo* evaluation of anti-psoriatic activity

Male BALB/c mice (8–10 weeks old) weighing 20–25 g were used to assess the optimised CRS-loaded ethosomal gel's in vivo anti-psoriatic efficacy. Before the experiment began, the animals were acquired from a CPCSEA-approved animal facility and acclimated to conventional laboratory settings for seven days. The Institutional Animal Ethics Committee (IAEC) approved the experimental protocol under approval number SDPC/IACE/2025/03. Every technique was performed in compliance with the standards set forth by the Government of India's Committee for Control and Supervision of Experiments on Animals (CPCSEA), as well as OECD guideline 404 for the evaluation of in vivo activity and ARRIVE reporting requirements. The animals were kept in a controlled environment with free access to a normal pellet meal and drinking water, at a temperature of 22 ± 2 °C, a relative humidity of 55 ± 10%, and a 12-hour light/dark cycle. All

experimental techniques were conducted in accordance with CPCSEA norms and the Institutional Animal Ethics Committee's (IAEC) permission[16].

As indicated in Table 1, the animals were split up into four experimental groups, each consisting of six individuals. All animals' dorsal skin was gently shaved without inflicting any harm twenty-four hours prior to illness induction (Day −1).

Throughout the trial period, no topical therapy nor disease induction were administered to the Normal group (Group 1). Topical administration of 62.5 mg of 5% Imiquimod cream over about 5 cm^2 of the shaved dorsal skin once daily in the morning for seven days in a row (Day 1 to Day 7) caused psoriasis-like skin lesions in the remaining groups[30].

Treatment began on Day 2 and lasted until Day 7, during which time imiquimod was used to induce illness every morning. The only therapy given to the animals in the disease control group (Group 2) was imiquimod cream. The marketed standard anti-psoriatic formulation (200 mg) was applied topically once a day in the evening to the animals in the Positive control group (Group 3). 200 mg of the optimised CRS-loaded ethosomal gel was applied topically once a day in the evening to the afflicted dorsal skin of the animals in the Treatment group (Group 4).

On Days 1, 2, 4, 6, and 7, body weight was measured. Erythema, scaling, and skin thickness were used to gauge the severity of psoriasis, and on Days 1, 2, 4, 6, and 7, the Psoriasis Area and Severity Index (PASI) score was computed. At the same intervals, a digital Vernier calliper was used to measure ear thickness (if suitable to your procedure).

All animals were put to sleep under anaesthesia on Day 8, and skin samples were taken for additional examination. For histopathological analysis using haematoxylin and eosin (H&E) staining, a portion of each skin sample was preserved in 10% neutral buffered formalin; the remaining tissue was kept at -80 °C to measure inflammatory cytokines and other biochemical data[31].

4. Results

4.1 Preformulation studies

To evaluate the physicochemical characteristics of CRS necessary for the creation of a stable and efficient topical ethosomal gel, preformulation tests were carried out. Preliminary information about the drug's properties and formulation appropriateness was given by these investigations. Organoleptic characterization, melting point determination, solubility analysis, and partition coefficient determination were all part of the evaluation[16].

4.1.1 Organoleptic Characterization

CRS was discovered to be a white, crystalline powder with a distinct smell. The drug's identity was confirmed and its appropriateness for further formulation development was indicated by the observed physical appearance, which matched the described features of the drug[32].

4.1.2 Melting Point Determination

The capillary method was used to determine the melting point of CRS. The claimed standard melting point range (128–134°C) and the actual melting point range (130–132°C) are quite similar. This verifies the drug's legitimacy and shows no appreciable impurities or deterioration[33].

4.1.3 Identification of CRS and Drug–Excipient Compatibility Study by FTIR

The structural identity and functional group integrity of CRS were verified using FTIR spectroscopy. The primary moieties of the molecule were represented by distinctive absorption bands in the spectra. The boronic acid group's O–H stretching vibration was identified as a large peak at 3317 cm^{-1}, and aromatic C–H stretching vibrations were identified as the band at 3060 cm^{-1}. The nitrile (C≡N) stretching vibration, a crucial structural indicator of CRS, was identified as the cause of the high absorption peak seen at 2225 cm^{-1}. Furthermore, the benzoxaborole framework's C–O–C stretching vibrations were linked to the absorption band at 1248 cm^{-1}. The drug's molecular validity was confirmed by the tight match between the reported spectral values and the observed frequencies. The drug sample's high purity and maintenance of chemical integrity are indicated by the lack of notable peak changes, the disappearance of distinctive bands, or the emergence of new peaks, all of which confirm the sample's appropriateness for formulation development. Before developing an ethosomal formulation, the compatibility of CRS with ethanol and cholesterol was evaluated using FT-IR spectroscopy. The physical mixture's spectra maintained the distinctive CRS absorption bands, indicating that the medication was still chemically stable when the chosen excipients were present. O–H stretching vibrations were identified as the cause of a wide band seen at 3518 cm^{-1}, indicating the presence of hydroxyl groups provided by both cholesterol and CRS. The drug molecule's aromatic framework was confirmed by the absorption peak at 2926 cm^{-1}, which correlated to aromatic C–H stretching vibrations. The significant peak at 1248 cm^{-1} was attributed to C–O–C stretching vibrations connected to the boron-containing molecular structure of CRS, whereas the distinctive nitrile stretching band (C≡N) was found at 2363 cm^{-1}. Notably, there

was no trace of peak disappearance, notable broadening, or the formation of new bands, and all of the drug's primary functional groups could still be identified within the physical mixture. Weak intermolecular interactions and changes in the microenvironment around the functional groups after mixing could be the cause of the small differences in peak positions when compared to reported values. Chemical incompatibility is not always indicated by such spectrum alterations, which are frequently seen in multicomponent systems. Overall, the FT-IR results show that CRS retains its structural integrity when ethanol and cholesterol are present, suggesting good drug–excipient compatibility. The successful creation of a stable and efficient ethosomal delivery system meant for improved topical medication administration depends critically on this compatibility[34]. **Figure:1** illustrate the (a) FTIR of CRS (b) FTIR of CRS +Ethanol+ Phospholipid (c) DSC studies of pure drug CRS.

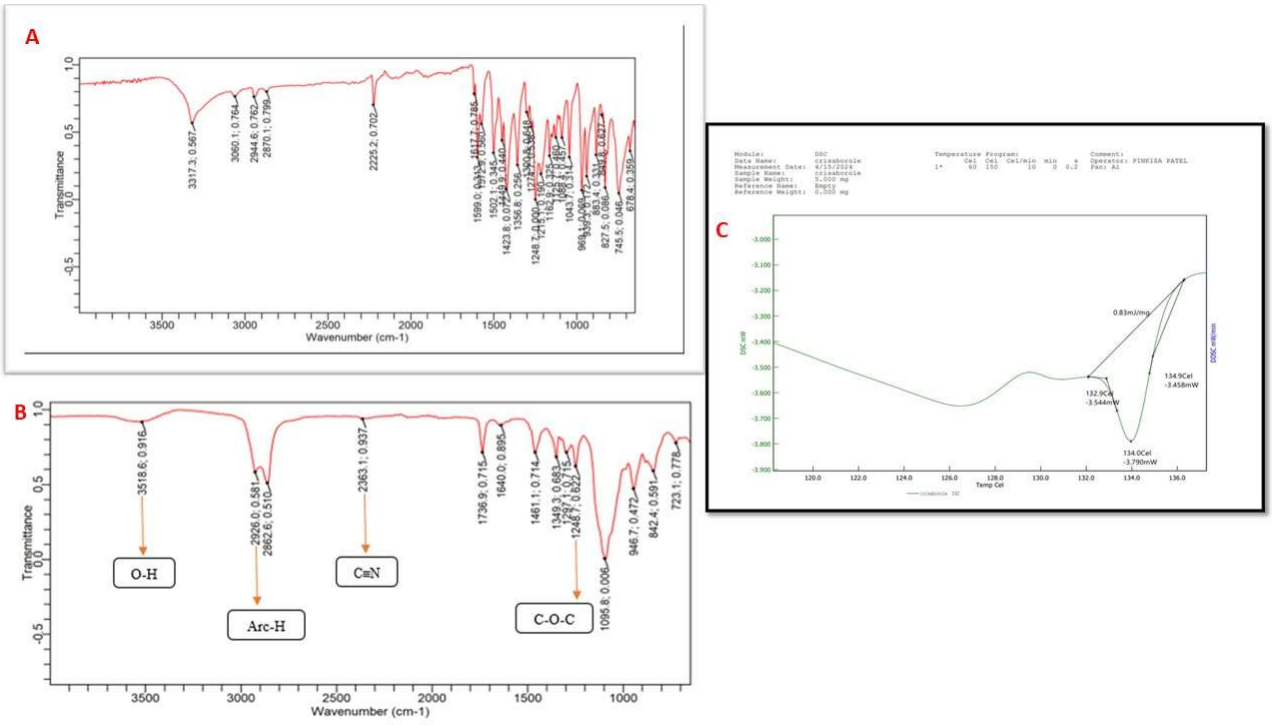

Figure:1 (a) FTIR of CRS (b) FTIR of CRS +Ethanol+ Phospholipid (c) DSC studies of pure drug CRS.

4.1.4 Solubility Study

In order to examine the dissolving properties of CRS and determine appropriate media for analytical evaluation and formulation development, solubility tests were carried out in a variety of solvents.

The findings confirmed that CRS is poorly hydrophilic and showed very little solubility in water (0.053 ± 0.04 mg/mL). On the other hand, better solubility was found in acidic and physiological conditions, with values of 2.47 ± 0.02 mg/mL in 0.1 N HCl and 2.54 ± 0.03 mg/mL in phosphate buffer (pH 7.4). CRS demonstrated considerable solubility in acetone (12.26 ± 0.038 mg/mL) and methanol (14.35 ± 0.04 mg/mL), indicating a significant increase in solubility in organic solvents. The drug molecule's lipophilic properties and higher affinity for non-aqueous environments are responsible for the increased solubilisation in organic mediums. According to the overall solubility profile, CRS is classified as poorly water-soluble, which may limit its bioavailability and dissolution. These results strongly support the creation of sophisticated vesicular carrier systems, such ethosomes, to enhance drug solubilisation, penetration, and topical medicinal efficacy[35].

4.2 Experimental Design and Optimization

Using a Box–Behnken Design (BBD), a systematic optimisation strategy based on a Quality by Design (QbD) approach was used to examine the impact of specific formulation variables on the physicochemical properties of CRS-loaded ethosomes. For optimisation, three crucial independent variables were chosen: sonication time (C), ethanol concentration (B), and cholesterol concentration (A). To ascertain their individual and combined effects on the vesicular system's properties, these formulation parameters were examined at three coded levels. Since these factors have a significant impact on vesicle performance, drug loading capacity, stability, and topical delivery behaviour, the produced formulations were assessed using three dependent responses: vesicle size (Y_1), entrapment efficiency (Y_2), and polydispersity index (Y_3). To determine the link between independent factors and observed responses, experimental data from the BBD runs were fitted to mathematical polynomial models. Analysis of variance (ANOVA) was used to determine the statistical significance of model terms and interaction effects. In order to provide a thorough knowledge of the impact of formulation variables on response characteristics, the developed response models were further evaluated using perturbation plots, contour plots, and three-dimensional response surface plots. Both individual factor effects and interaction patterns within the design space might be seen thanks to these graphical representations. A desire function technique was used to optimise the formulation with the goal of maximising entrapment efficiency while minimising vesicle size and PDI. The experimental design matrix and related responses for CRS-loaded ethosomal formulations are shown in **Table 3[36]**. **Table 4** summarises the model selection and statistical adequacy parameters for the assessed responses. While Figure 3 (A–C)

shows the three-dimensional response surface plots illustrating the effects of ethanol and cholesterol concentration on vesicle size, entrapment efficiency, and PDI of CRS-loaded ethosomes, **Figure 2** (A–C) shows the perturbation plots describing the influence of formulation variables on the investigated responses. The BBD matrix and observed responses for the optimisation of CRS-loaded ethosomes are shown in Table 3.

Table:3 Box–Behnken Experimental Design Matrix and Observed Responses for the Optimization of Crisaborole-Loaded Ethosomes

Run	Cholesterol (mg)	Ethanol (%)	Sonication Time (min)	Vesicle Size (nm)	Entrapment Efficiency (%)	PDI
1	**3**	**40**	**10**	219.1 ± 1.8	88.87 ± 0.76	0.28 ± 0.02
2	**3**	**20**	**10**	248.0 ± 2.3	83.65 ± 0.68	0.22 ± 0.01
3	**1**	**30**	**5**	161.5 ± 1.2	68.43 ± 0.52	0.18 ± 0.01
4	**3**	**30**	**5**	237.5 ± 2.1	84.42 ± 0.73	0.25 ± 0.02
5	**2**	**40**	**15**	132.4 ± 1.0	73.88 ± 0.61	0.30 ± 0.02
6	**1**	**20**	**10**	185.0 ± 1.5	68.93 ± 0.57	0.16 ± 0.01
7	**2**	**20**	**5**	187.8 ± 1.7	70.12 ± 0.63	0.20 ± 0.01
8	**2**	**40**	**5**	140.9 ± 1.1	72.18 ± 0.58	0.27 ± 0.02
9	**1**	**40**	**10**	130.6 ± 0.9	67.92 ± 0.49	0.24 ± 0.01
10	**1**	**30**	**15**	149.7 ± 1.3	65.46 ± 0.46	0.21 ± 0.01
11	**2**	**30**	**10**	170.2 ± 1.6	74.82 ± 0.66	0.19 ± 0.01
12	**2**	**20**	**15**	192.9 ± 1.9	71.08 ± 0.55	0.23 ± 0.01
13	**3**	**30**	**15**	212.3 ± 2.0	85.48 ± 0.81	0.29 ± 0.02

Footnote: Cholesterol concentration (X_1), ethanol concentration (X_2), and sonication time (X_3) were investigated at three levels using a Box–Behnken design. Vesicle size, entrapment efficiency, and polydispersity index (PDI) are expressed as mean ± standard deviation (SD) (n = 3). Abbreviations: PDI, polydispersity index; SD, standard deviation.

4.3 Interpretation of the Polynomial Equation for Vesicle Size (Y_1)

The effect of the selected formulation variables on vesicle size (Y_1) was adequately represented by the fitted quadratic polynomial equation. In terms of coded factors, the model is expressed as:

$$\mathbf{Y1 = 167.72 + 36.26X_1 - 23.84X_2 - 5.05X_3 + 6.38X_1X_2 - 3.35X_1X_3 - 3.40X_2X_3 + 26.11X_1^2 - 0.6375X_2^2 - 6.06X_3^2}$$

where X_1 represents cholesterol concentration, X_2 represents ethanol concentration, X_3 represents sonication time, and Y_1 represents vesicle size (nm). The intercept value of 167.72 nm represents the predicted vesicle size at the centre point of the experimental design. Among the linear terms, cholesterol concentration exhibited the strongest positive effect (+36.26), indicating that increasing cholesterol concentration tended to increase vesicle size. This may be associated with enhanced bilayer rigidity and increased membrane thickness, which can promote the formation of larger vesicular structures. In contrast, ethanol concentration showed a pronounced negative effect (−23.84), possibly because ethanol increases membrane fluidity and deformability, facilitating vesicle reorganization and size reduction. Sonication time also produced a negative effect (−5.05), consistent with the mechanical disruption of larger vesicles into smaller structures. The positive X_1X_2 interaction (+6.38) suggests that the combined influence of cholesterol and ethanol partially counteracted their individual effects, reflecting the balance between membrane rigidity and fluidity[37]. The negative X_1X_3 and X_2X_3 interactions indicate that sonication may enhance the size-reducing effects of these formulation variables. The substantial positive quadratic coefficient for cholesterol (+26.11) confirms a marked nonlinear effect, suggesting that excessive cholesterol may cause a disproportionate increase in vesicle size. Conversely, the negative quadratic terms for ethanol and sonication indicate a tendency toward size reduction within the studied range. Overall, the model demonstrates that cholesterol concentration was the dominant determinant of vesicle size, while ethanol concentration and sonication provided important size-reducing effects[27].

4.4 Interpretation of the Polynomial Equation for Entrapment Efficiency (EE) (Y_2)

The relationship between the formulation variables and the EE of the optimized ethosomal formulation was described by the following quadratic polynomial equation in coded factors:

$$\mathbf{Y2 = 73.90 + 8.96X_1 + 1.13X_2 + 0.0937X_3 + 1.56X_1X_2 + 1.01X_1X_3 + 3.67X_1^2 - 1.86X_3^2}$$

where X_1 represents cholesterol concentration, X_2 represents ethanol concentration, X_3 represents sonication time, and Y_2 represents entrapment efficiency (%). The intercept value (73.90) represents the predicted EE at the centre point of the experimental design. Among the linear terms, cholesterol concentration showed the strongest positive influence (+8.96), indicating that it was the principal factor governing drug entrapment. This effect may be attributed to the ability of cholesterol to enhance bilayer packing and membrane rigidity, thereby reducing drug leakage and improving

retention of the lipophilic drug within the ethosomal structure. Ethanol concentration also showed a positive effect (+1.13), possibly because moderate ethanol levels enhance membrane fluidity and facilitate drug incorporation into the lipid domain. The relatively small positive coefficient for sonication time (+0.0937) suggests a limited beneficial effect within the investigated range, potentially due to improved vesicle dispersion and structural homogenization. The positive interaction terms (X_1X_2 and X_1X_3) indicate that cholesterol acted synergistically with ethanol and sonication to enhance drug entrapment. The positive quadratic coefficient for cholesterol (+3.67) indicates a nonlinear contribution, whereas the negative quadratic coefficient for sonication time (−1.86) suggests that excessive sonication may compromise vesicle integrity and promote drug leakage. Overall, the model identifies cholesterol concentration as the dominant determinant of EE and emphasizes the need to balance membrane rigidity, fluidity, and processing energy to maximize drug loading while maintaining vesicle stability[38].

4.5 Interpretation of the Polynomial Equation for Polydispersity Index (Y_3)

The relationship between the formulation variables and the polydispersity index (PDI) of the optimized ethosomal formulation was represented by the following quadratic polynomial equation in coded factors:

$$\boldsymbol{Y3 = 2.00 + +0.0312X_1 0.0350X_2 + 0.0162X_3 + 0.0225X_2^2 + 0.03X_3^2}$$

The quadratic polynomial equation in coded factors was used to characterise the relationship between the formulation variables and the polydispersity index (PDI) of the optimised ethosomal formulation. In this case, X_1 stands for the concentration of cholesterol, X_2 for ethanol, X_3 for sonication time, and $Y\infty$ for PDI. The projected PDI in the experimental design's center, where all independent variables are kept at their coded zero levels, is represented by the intercept value of 0.2000. The linear terms that contributed most to PDI were ethanol concentration (+0.0350), followed by cholesterol concentration (+0.0312) and sonication time (+0.0162). The positive coefficients indicate that vesicle-size heterogeneity tended to rise as these factors were increased within the studied design space. Further evidence of nonlinear behaviour is provided by the positive quadratic coefficients for ethanol concentration (+0.0225) and sonication time (+0.0300), which imply that high concentrations may gradually widen the particle-size distribution. Excessive fluidisation of the phospholipid bilayer, which might compromise vesicle integrity and encourage size fluctuation, may be linked to the rise in PDI with ethanol concentration. Higher cholesterol levels can also alter the packing and rigidity of bilayers, which can lead to the creation of

heterogeneous vesicles[39]. Since prolonged sonication may result in excessive fragmentation followed by vesicle reorganisation or re-association, the effect of sonication probably reflects a balance between size reduction and structural disruption. Sonication time had a significant contribution through its nonlinear effect, but ethanol content overall had the biggest linear influence. In order to achieve a homogenous ethosomal dispersion with a limited size distribution and enhanced physical stability, these results emphasise the significance of striking a balance between membrane fluidity, bilayer rigidity, and sonication energy[40]. **Figure:2 Optimization plots illustrating the influence of formulation variables on the responses of the optimized ethosomal formulation. (a) Perturbation plot for vesicle size, (b) perturbation plot for entrapment efficiency, (c) perturbation plot for polydispersity index (PDI), (d) three-dimensional response surface plot for vesicle size, (e) three-dimensional response surface plot for entrapment efficiency, and (f) three-dimensional response surface plot for PDI.**

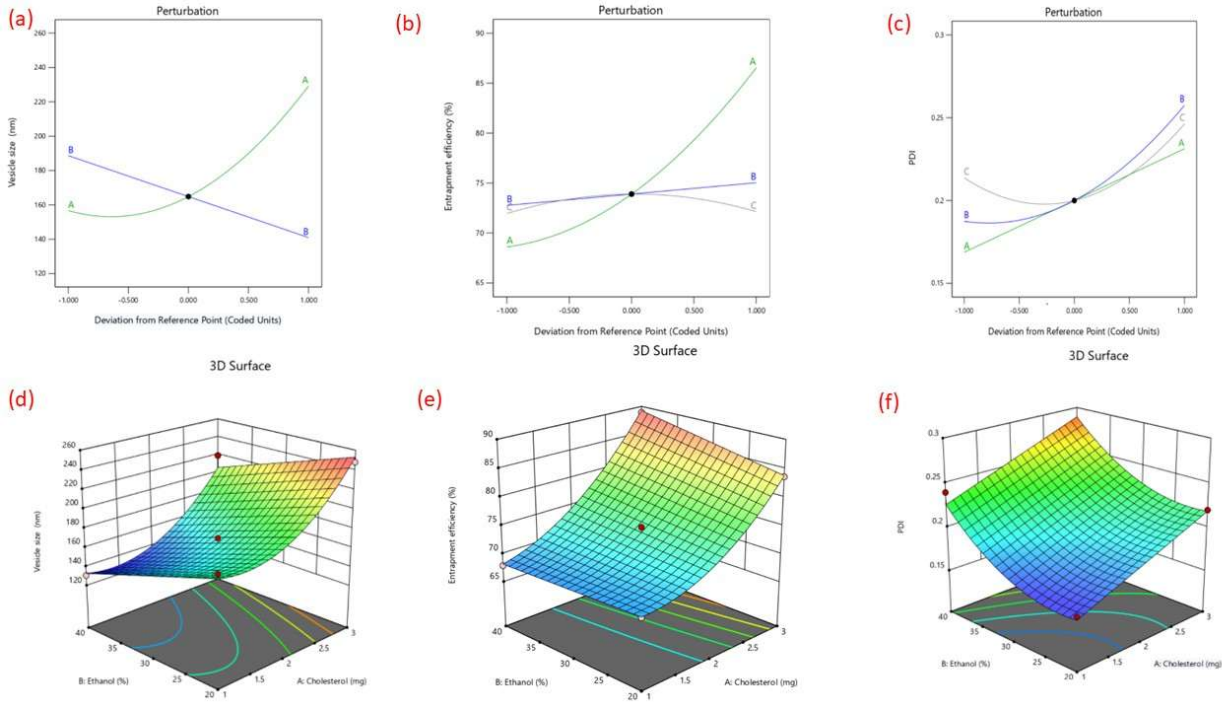

Figure:2 Optimization plots illustrating the influence of formulation variables on the responses of the optimized ethosomal formulation. (a) Perturbation plot for vesicle size, (b) perturbation plot for entrapment efficiency, (c) perturbation plot for polydispersity index (PDI), (d) three-dimensional response surface plot for vesicle size, (e) three-dimensional

response surface plot for entrapment efficiency, and (f) three-dimensional response surface plot for PDI.

4.6 Selection of the Optimized CRS-Loaded Ethosomal Formulation

The formulation was optimised using the Box-Behnken design (BBD), which assessed the impact of ethanol concentration (X_2), cholesterol concentration (X_1), and sonication time (X_3) on vesicle size, entrapment efficiency (EE), and polydispersity index (PDI). Significant linear and nonlinear impacts of the formulation factors were confirmed using quadratic models, which properly characterised all answers. The constructed models had high predictive capacity within the experimental design space, as evidenced by their satisfactory statistical performance.

The goal of numerical optimisation was to maximise entrapment efficiency while minimising vesicle size and PDI utilising Design-Expert®'s desirability function. The optimal formulation, which offers the optimum balance between vesicle homogeneity, physicochemical stability, and drug loading, was chosen based on the highest attractiveness value. The ideal ratio of ethanol, cholesterol, and sonication duration resulted in nanosized, evenly dispersed ethosomes with high drug encapsulation, which are advantageous for improved formulation stability and skin penetration.

For validation, the optimised formulation was made in triplicate. With prediction errors less than 5%, the experimentally observed values for vesicle size, PDI, and entrapment efficiency nearly matched the expected values, demonstrating the precision and resilience of the optimisation model. These results show that the ideal CRS-loaded ethosomal formulation has the physicochemical properties needed for effective topical medication administration. **Table:4** illustrate the check point analysis for optimized CRS -loaded ethosomal formulation. **Figure 2.** DLS and TEM characterization of optimized CRS-loaded ethosomal formulations. (a) DLS size distribution of CE1; (b) TEM image of CE1; (c) TEM image of CE2; and (d) DLS size distribution of CE2

Table:4 Check point analysis for optimized CRS -loaded ethosomal formulation

Selected	Desirability	Dependent Variables			Predicted responses			Experimental Responses		
		X1 (mg)	X2 (%)	X3 (Minute)	Y1	Y2	Y3	Y1	Y2	Y3

CE1	**1**	2.36	30.18	9.216	181.47	77.59	0.210	18 1.3	80	0.284
CE2	**1**	2.38	30.7	7.98	181.48	77.56	0.213	18 5	76	0.332

4.7 Optimized CRS-loaded ethosomes characterization

Vesicle size, polydispersity index (PDI), and entrapment efficiency were used to assess the physicochemical properties of the optimised CRS (CRS)-loaded ethosomal formulations because these factors have a significant impact on vesicular stability, skin penetration, and overall therapeutic efficacy. Two optimised checkpoint formulations (CE1 and CE2) with a desirability value of 1.0 were created utilising the optimised factor levels in order to verify the predictive power of the Box-Behnken design (BBD). The appropriate values predicted by the optimisation model were then compared to the experimental responses. In contrast to the experimentally obtained particle sizes of 181.3 nm and 185 nm, the optimisation model predicted vesicle sizes of 181.47 nm and 181.48 nm for CE1 and CE2, respectively. The created quadratic model's good predictability is demonstrated by the close agreement between the observed and anticipated values, which also validates the optimisation approach's dependability. The observed small variance (<3%) indicates the robustness and reproducibility of the formulation process and is within acceptable experimental bounds. Because vesicle size controls skin penetration, drug deposition, and vesicular stability, it is a crucial factor in determining how well topical nanocarriers work. The successful creation of nanosized ethosomal vesicles was demonstrated by both optimised formulations' particle sizes being less than 200 nm. These nanoscale vesicles are more deformable and may more efficiently pass through the stratum corneum's intercellular lipid matrix, which increases medication accumulation in psoriatic lesions while lowering systemic exposure. As a result, it is anticipated that the optimised particle size will boost therapeutic efficacy and localised administration of CRS. By calculating the polydispersity index (PDI), the homogeneity of the vesicular dispersions was evaluated. The experimentally determined values were 0.284 and 0.332, respectively, whereas the optimisation model anticipated PDI values of 0.210 for CE1 and 0.213 for CE2. The tight agreement between the expected and observed outcomes attests to the optimisation model's suitability. Additionally, a narrow particle-size distribution is indicated by PDI values less than 0.30, which represent the development of a homogeneous vesicular population with little aggregation. By

efficiently converting bigger vesicles into uniformly distributed nanosized particles, the optimised sonication period made a substantial contribution to the achievement of homogenous vesicle dispersion. To ascertain if the optimised ethosomal system could hold CRS inside the phospholipid bilayer, entrapment efficiency was assessed. While the experimental values were 80% and 76%, the anticipated entrapment efficiencies for CE1 and CE2 were 77.59% and 77.56%, respectively. The accuracy of the optimisation model is further supported by the strong agreement between the predicted and experimental responses. The optimal combination of phospholipid concentration, ethanol content, cholesterol, and sonication conditions, which together supported stable vesicle formation and effective drug integration, is responsible for the high encapsulation efficiency. Cholesterol reduces medication leakage and increases bilayer stiffness[41], whereas ethanol imparts membrane flexibility, facilitating the formation of stable ethosomal vesicles with high drug-retention capacity[42]. The validity and robustness of the Box-Behnken optimisation model were confirmed by the checkpoint analysis, which showed excellent agreement between the predicted and experimental responses for vesicle size, PDI, and entrapment efficiency. A stable and effective topical nanocarrier system for improved skin administration of CRS in psoriasis treatment was demonstrated by the optimised CRS-loaded ethosomal formulations, which showed nanosized vesicles, a limited particle-size distribution, and excellent drug encapsulation[43].

4.8 Transmission Electron Microscopy (TEM) Analysis

The optimised CRS-loaded ethosomal formulation's shape and structural features were examined using TEM. The generated ethosomes were primarily spherical to nearly spherical in shape with clearly defined vesicular borders, according to representative TEM micrographs. The vesicles successfully formed stable nanosized vesicles because they were evenly dispersed and showed no signs of aggregation or structural collapse[44].

Although the vesicles appeared somewhat smaller because DLS measures the hydrodynamic diameter in an aqueous solution whereas TEM measures the dehydrated state of the particles, the particle size shown in the TEM pictures was comparable with the results of dynamic light scattering (DLS). The intact phospholipid bilayer and smooth vesicular surface indicate that the chosen formulation factors supplied sufficient membrane stability throughout the preparation procedure. The lack of fused or asymmetrically formed vesicles provides additional evidence that the ideal formulation conditions were successful in creating a homogenous ethosomal dispersion[45]. These morphological results show that the optimised CRS-loaded ethosomes are suitable as a stable

nanovesicular carrier for topical drug administration and corroborate the particle size, PDI, and entrapment efficiency results[46]. **Figure:3 DLS and TEM characterization of optimized CRS-loaded ethosomal formulations. (a) DLS size distribution of CE1; (b) TEM image of CE1; (c) TEM image of CE2; and (d) DLS size distribution of CE2.**

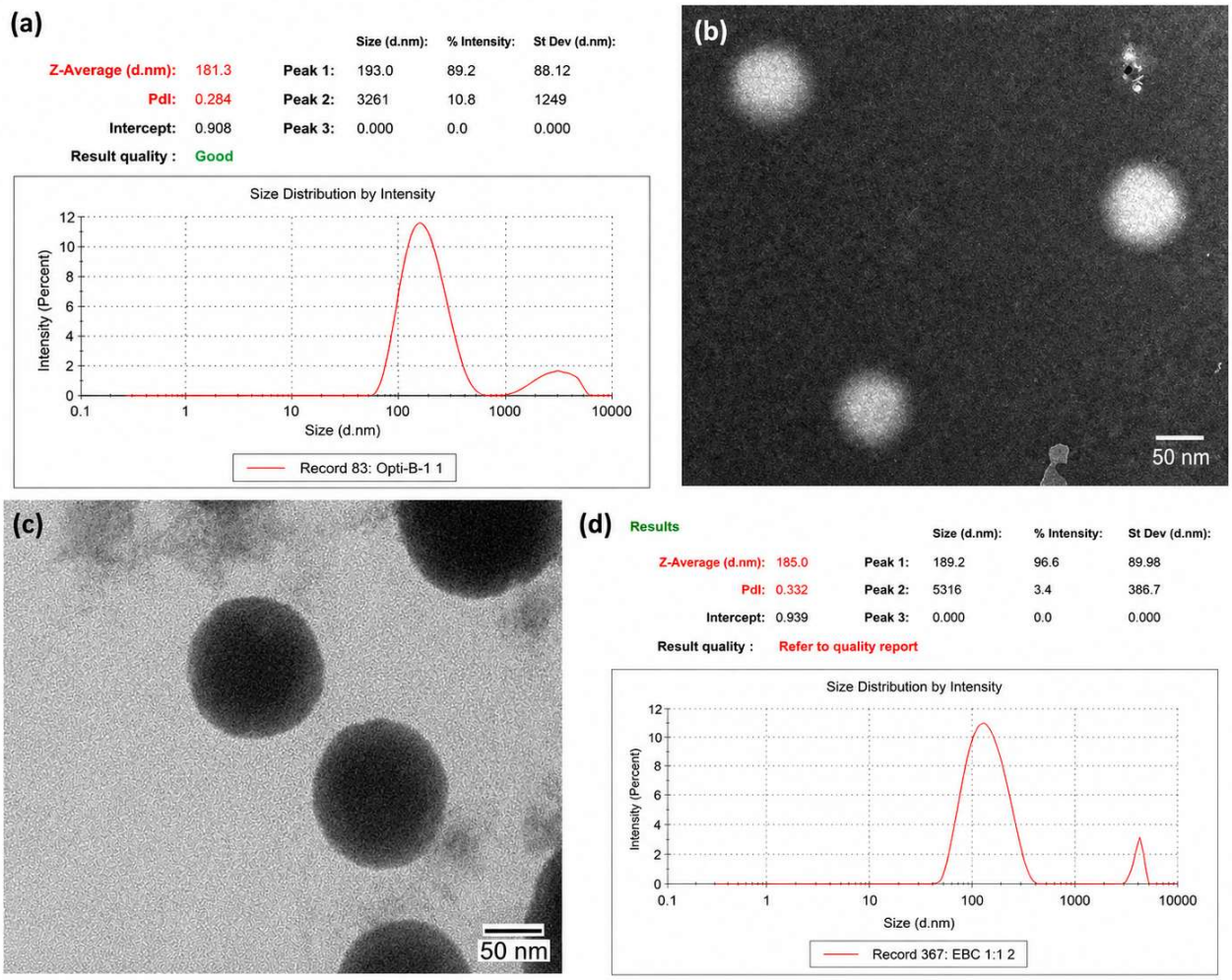

4.9 *In Vitro* Drug Release Study

To ascertain the impact of vesicular encapsulation on drug release and to clarify the primary release mechanism, the in vitro release behaviour of CRS from the optimised ethosomal formulation (CE1) was compared with the pure drug suspension. The pure CRS suspension demonstrated quick drug liberation, with around 40% release in 1 hour and almost full release by 2 hours, as seen in Figure 4(a). With cumulative drug release of roughly 15.3% at 1 hour, 31.5% at 2 hours, 41.0% at 3 hours, 53.2% at 4 hours, 59.1% at 5 hours, 61.7% at 6 hours, and 65.0% at 7 hours, CE1, on the other hand, showed a progressive and persistent release pattern. The release then rose to 71.8% at 8 hours,

75.2% at 9 hours, 79.1% at 10 hours, 83.2% at 11 hours, and 85.0% at 12 hours. As a result, while the pure drug suspension released nearly all of the medication during the first two hours, the ethosomal formulation prolonged CRS release over a period of twelve hours. This clear distinction shows how the ethosomal system can control medication availability and lessen the unencapsulated drug's fast release[16].

The structural features of the vesicular carrier are responsible for the extended release profile of CE1. Before entering the external release media, CRS integrated into or connected to the phospholipid bilayer must diffuse via the organised lipid domain. While ethanol alters bilayer fluidity and promotes regulated molecular transport, cholesterol may support membrane organization and structural integrity. When these elements work together, they can produce a diffusional barrier that prevents drug release while preserving enough membrane flexibility for gradual release. Therefore, the presence of both easily accessible drug fractions and drug held within the vesicular structure is suggested by the release pattern, which is characterised by an initial phase followed by a slower and longer phase[47].

The experimental data were fitted to zero-order, first-order, Higuchi, and Korsmeyer–Peppas kinetic models in order to further describe the release behaviour. The zero-order model indicated a coefficient of determination of R2 = 0.9238 and a progressive rise in cumulative drug release over time. The first-order model showed a relatively weaker association (R2 = 0.7391), suggesting that the concentration of medication remaining in the formulation was insufficient to describe release. A higher correlation (R^2 = 0.9663) was obtained from the Korsmeyer–Peppas model, indicating that diffusional transport contributes to CRS release. Nonetheless, the Higuchi model was deemed the best-fitting model among those assessed since it displayed the highest correlation, with R2 = 0.9867. Diffusion was the main mechanism controlling CRS release from CE1, according to the Higuchi model's better fit. The slow-release profile and the ethosomal bilayer's function as a diffusional reservoir are compatible with this theory. Diffusion's contribution is further supported by the excellent correlation found with the Korsmeyer-Peppas model; nevertheless, a mechanistic interpretation of this model should also take the computed release exponent (n) into account. Overall, the kinetic analysis shows that CE1 significantly altered the free CRS's quick release behavior and produced a protracted release profile that lasted for almost 85% throughout a 12-hour period. Because they keep the medication available at the application site for a longer amount of time, these features may be beneficial for topical delivery. The other kinetic models offer

complementary evidence about the release behavior of the optimized ethosomal formulation, but the Higuchi model should be considered the primary mathematical description of the current release data[48]. **Figure:4** illustrate the i*n vitro* drug release kinetics and mathematical modeling of optimized formulation of CRS-loaded ethosomes (CE1).

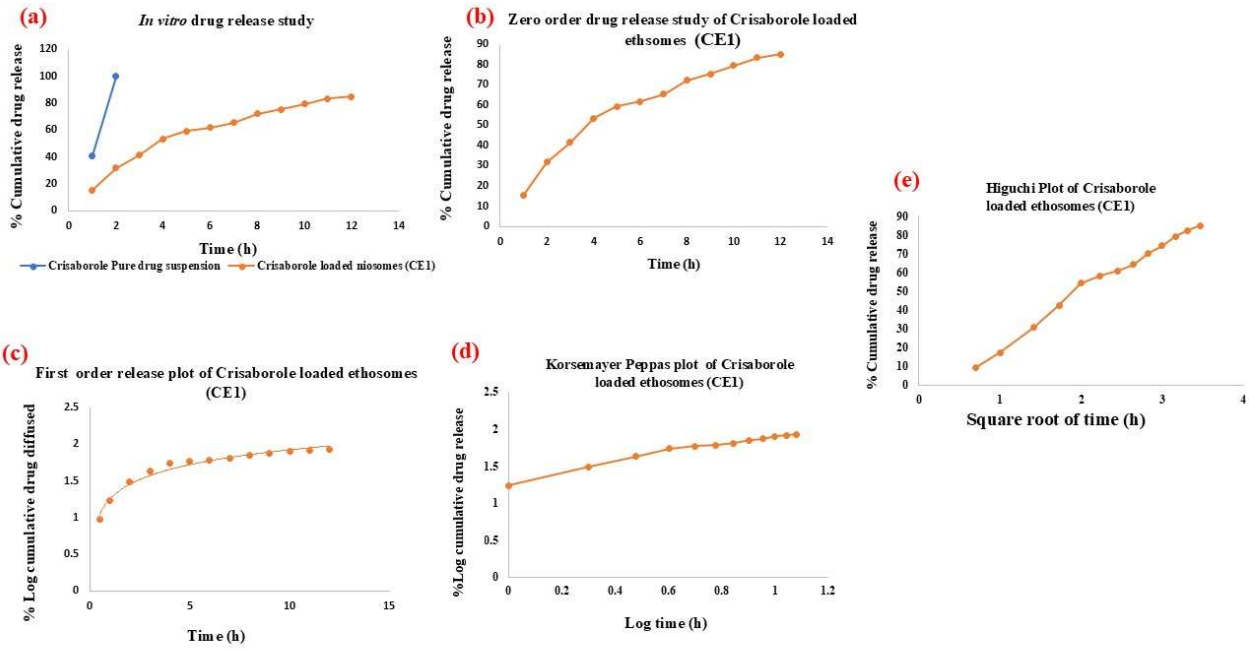

Figure:4 *In vitro* drug release kinetics and mathematical modeling of optimized formulation of CRS-loaded ethosomes (CE1).

5. *In vivo* evaluation of anti-psoriatic activity

5.1 Effect of treatment on PASI score

Over the course of the study, topical imiquimod application caused the disease-control group's PASI score to gradually rise. Psoriasis-like skin lesions progressively developed, as evidenced by the score rising from 0.83 ± 0.75 on Day 1 to 4.00 ± 0.00 on Day 7. On the other hand, following treatment, the positive-control group's PASI score significantly decreased, going from 2.50 ± 0.55 on Day 4 to 0.83 ± 0.75 on Day 7. The PASI score dropped from 2.33 ± 0.52 on Day 4 to 1.00 ± 0.89 on Day 7, indicating a similar therapeutic effect from the optimised CRS-loaded ethosomal gel. Throughout the trial, the normal-control group's score remained at zero. These results suggest that imiquimod-induced psoriasiform skin inflammation was significantly reduced by treatment with the optimised ethosomal gel. The Psoriasis Area and Severity Index (PASI) scores for the

normal, disease control, standard, and therapy groups are shown in **Figure 5 Panels (a–e)** from Day 1 to Day 7. The standard and treatment groups dramatically decreased the severity of the disease over time, showing successful suppression of IMQ-induced psoriatic lesions, while the disease control group showed a steady increase in PASI score.[49].

5.2 Effect on ear thickness

Inflammatory tissue swelling was seen in the disease-control group, whose ear thickness increased significantly from 0.22 ± 0.02 mm on Day 1 to 0.46 ± 0.06 mm on Day 7. On Day 7, the positive-control group showed a lesser rise of 0.31 ± 0.03 mm. Among the imiquimod-treated groups, the optimised CRS-loaded ethosomal gel showed the least increase; on Day 7, ear thickness measured 0.26 ± 0.05 mm, which was near the normal-control value of 0.22 ± 0.05 mm. These findings show a significant reduction in tissue thickness linked to inflammation after treatment[50]. **Figures 5 (f) and (g)** illustrate the ear thickness of mice measured on Day 1 and Day 7, respectively, following IMQ-induced psoriasis. The optimized Crisaborole-loaded ethosomal gel significantly reduced ear swelling by Day 7 compared with the disease control group, indicating effective suppression of psoriatic inflammation and edema.

5.3 Effect on body weight

The body weight of the disease-control group decreased from 22.33 ± 1.21 g on Day 1 to 19.17 ± 1.17 g on Day 7. The optimised therapy group, on the other hand, changed from 22.50 ± 1.52 g to 22.67 ± 0.82 g over the same time period, maintaining a relatively stable body weight. While the normal-control group exhibited a modest increase, the positive-control group showed a slight decrease from 22.17 ± 0.75 g to 21.83 ± 0.41 g. The therapy group's ability to maintain body weight throughout the trial duration indicates favourable overall tolerability. **Figure: 5 Panels (f–g)** depict ear thickness measurements on Days 1 and 7 as an indicator of cutaneous inflammation. Ear thickness remained comparable among all groups on Day 1; however, by Day 7, the disease control group showed a marked increase, while both the standard and treatment groups exhibited a substantial reduction in ear thickness, demonstrating their anti-inflammatory efficacy against psoriasis-associated edema[51].

5.4 Effect on spleen weight

Spleen weight was significantly higher in the disease-control group (0.198 ± 0.017 g) than in the normal-control group (0.078 ± 0.010 g). The optimised CRS-loaded ethosomal gel resulted in a further reduction to 0.105 ± 0.010 g, while the marketed standard treatment lowered spleen weight

to 0.138 ± 0.025 g. The optimized-treatment group's significantly decreased spleen weight suggests a reduction in the systemic immune response linked to imiquimod-induced inflammation[51]. **Figure 5(h)** illustrates the spleen weight of mice measured on Day 7 following IMQ-induced psoriasis. Treatment with the optimized Crisaborole-loaded ethosomal gel markedly reduced spleen enlargement compared with the disease control group, indicating attenuation of systemic inflammation and improved therapeutic efficacy.

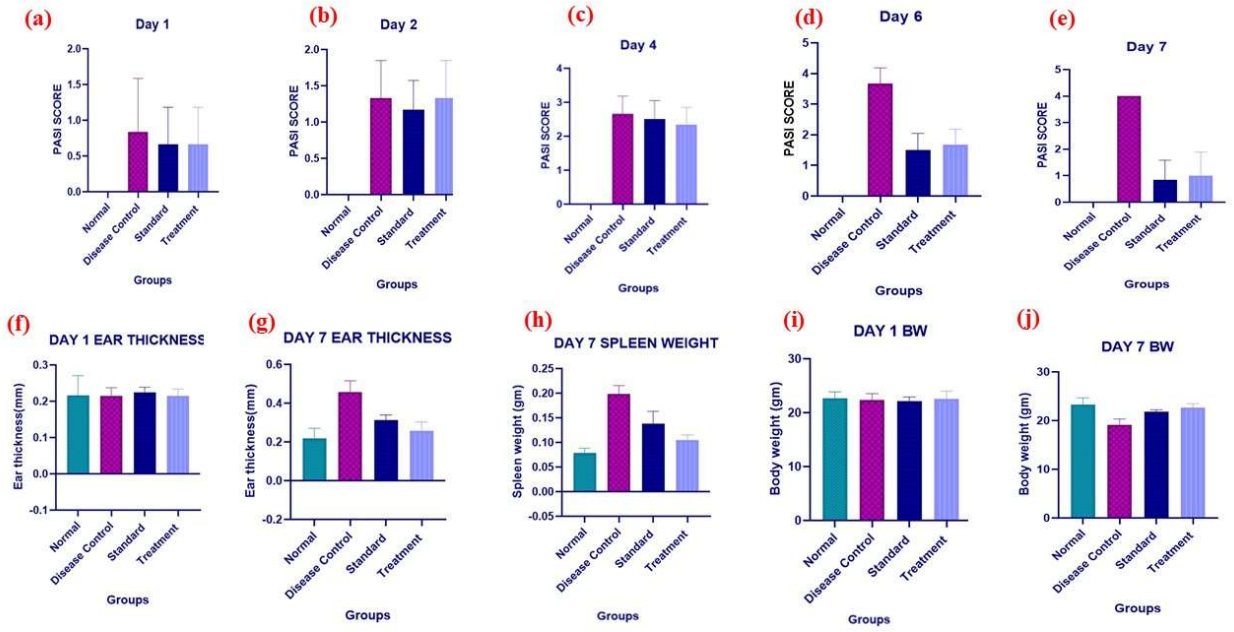

Figure:5 *In vivo* evaluation of the anti-psoriatic efficacy of the optimized Crisaborole-loaded ethosomal gel in the imiquimod (IMQ)-induced psoriasis mouse model. (a) Psoriasis Area and Severity Index (PASI) score on Day 1, (b) PASI score on Day 2, (c) PASI score on Day 4, (d) PASI score on Day 6, (e) PASI score on Day 7, (f) Ear thickness on Day 1, (g) Ear thickness on Day 7, (h) Spleen weight measured on Day 7, (i) Body weight recorded on Day 1, and (j) Body weight recorded on Day 7. Data are expressed as mean ± SD (n = 6). Experimental groups comprised the Normal control, Disease control (IMQ-induced psoriasis), Standard treatment, and Optimized Crisaborole-loaded ethosomal gel treatment groups. The optimized formulation significantly reduced PASI scores, ear thickness, and spleen weight while preventing disease-associated body weight loss, demonstrating its therapeutic potential against IMQ-induced psoriatic skin inflammation.

5.5 Effect on inflammatory cytokines

The injection of imiquimod resulted in a significant rise in both assessed inflammatory mediators. In the disease-control group, IL-6 rose from 44.67 ± 3.06 pg/mg protein to 70.33 ± 2.08 pg/mg protein. The optimised CRS-loaded ethosomal gel yielded a result of 58.67 ± 1.53 pg/mg protein, whereas treatment with the standard formulation decreased the amount to 54.67 ± 3.06 pg/mg protein. For IL-22, a more noticeable change was noted. After imiquimod was administered, the IL-22 concentration significantly rose from 73.67 ± 1.15 pg/mg protein in the normal-control group to 452.67 ± 3.79 pg/mg protein. Treatment decreased IL-22 to 107.67 ± 6.43 pg/mg protein with the optimised ethosomal gel and 110.67 ± 4.93 pg/mg protein with the positive control. As a result, the optimised formulation significantly decreased the rise of IL-22 caused by imiquimod and brought it back to a level that was comparable to that seen in the group receiving normal treatment[52]. **Figures:6** (a) and (b) illustrate the levels of the pro-inflammatory cytokines IL-6 and IL-22, respectively, in skin tissue homogenates of mice with IMQ-induced psoriasis. Treatment with the optimized Crisaborole-loaded ethosomal gel significantly reduced IL-6 and IL-22 levels compared with the disease control group, indicating attenuation of psoriasis-associated inflammatory responses.

5.6 Histopathological evaluation

The macroscopic and biochemical results were validated by histological analysis. Skin sections from the normal-control group revealed no discernible inflammatory infiltration and a thin, well-organised epidermis with a regular dermoepidermal junction. The development of psoriasis-like clinical alterations was confirmed by the disease-control group, which showed significant epidermal thickness, severe acanthosis, considerable surface hyperkeratosis, and widespread inflammatory-cell infiltration.

When compared to the disease-control group, the positive-control group had less inflammatory infiltration and less epidermal thickening, indicating a partial restoration of the epidermal architecture. More noticeable tissue healing was achieved by the optimised CRS-loaded ethosomal gel, which was marked by a significant decrease in inflammatory cell infiltration and epidermal hyperplasia as well as an improvement in the overall dermal architecture. All of the histopathological results point to the optimised formulation's ability to prevent imiquimod-induced cutaneous inflammatory alterations[53]. **Figures 6 (c–f)** illustrate the representative hematoxylin and eosin (H&E)-stained histopathological sections of skin from the Normal control (Group 1),

Disease control (Group 2), Standard treatment (Group 3), and Optimized Crisaborole-loaded ethosomal gel treatment (Group 4), respectively. The optimized formulation markedly restored normal skin architecture by reducing epidermal hyperplasia, hyperkeratosis, and inflammatory cell infiltration compared with the disease control group, demonstrating significant histopathological improvement.

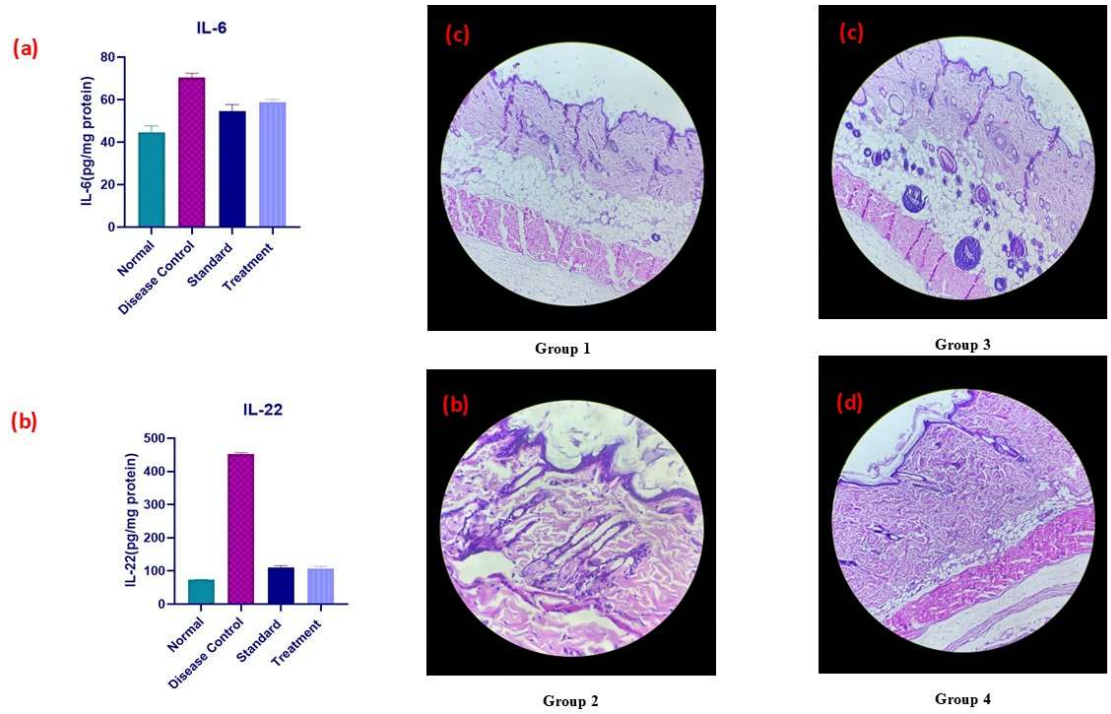

Figure:6 Effect of the optimized Crisaborole-loaded ethosomal gel on inflammatory cytokine levels and histopathological changes in the imiquimod (IMQ)-induced psoriasis mouse model. (a) IL-6 concentration in skin tissue homogenates, (b) IL-22 concentration in skin tissue homogenates, (c) Histopathological section of the Normal control (Group 1) showing intact epidermal architecture and normal skin morphology, (d) Histopathological section of the Disease control (Group 2) showing marked epidermal hyperplasia, hyperkeratosis, inflammatory cell infiltration, and psoriatic lesions, (e) Histopathological section of the Standard treatment (Group 3) showing partial restoration of normal skin architecture with reduced epidermal thickening and inflammation, and (f) Histopathological section of the Optimized Crisaborole-loaded ethosomal gel treatment (Group 4) showing near-normal epidermal morphology with minimal inflammatory infiltration and significant improvement in psoriatic lesions. Data are presented as mean ± SD (n = 6 per group). Histological sections were stained with hematoxylin and eosin (H&E).

6. Discussion

The creation of a QbD-guided CRS-loaded ethosomal system for topical psoriasis treatment was successfully demonstrated in this work. Vesicle size, EE, and PDI were all determined by the combination of cholesterol concentration, ethanol content, and sonication time, as demonstrated by the Box-Behnken design, which successfully showed the association between formulation factors and important quality attributes. The robustness and dependability of the optimisation model were confirmed by the strong agreement between the expected and experimental responses, which supported the use of QbD for creating repeatable nanovesicular formulations[54].

Cholesterol improved drug entrapment and increased vesicle size due to increased membrane stiffness, making it the variable that had the biggest impact on vesicle properties among those examined. On the other hand, optimised sonication resulted in homogenous nanosized vesicles with no aggregation, while ethanol decreased vesicle size by increasing phospholipid bilayer fluidity and deformability. With a vesicle size of about 181 nm, low PDI, and high EE (~80%), the optimised formulation demonstrated a stable and evenly distributed nanocarrier appropriate for improved cutaneous distribution. Similar findings have been documented for ethosomal formulations, where vesicle stability, drug loading, and skin penetration efficiency are determined by the equilibrium between membrane rigidity and flexibility[55].

In contrast to the quick release of the pure drug suspension, the optimised ethosomes also generated continuous CRS release throughout a 12-hour period. The Higuchi model's better fit indicated that cholesterol helped stabilise the membrane and prevent premature drug leakage, whereas drug release was mostly diffusion-controlled across the phospholipid bilayer. Because it sustains therapeutic drug concentrations at the application site, such extended drug release is beneficial for topical psoriasis treatment, potentially lowering dosage frequency and enhancing patient compliance[56].

In the imiquimod-induced psoriasis model, the improved physicochemical characteristics resulted in notable biological effectiveness. PASI score, ear thickness, spleen weight, IL-6, and IL-22 levels were significantly decreased by treatment with the optimised CRS-loaded ethosomal gel, and histological analysis revealed that normal skin architecture had been restored[57]. These results suggest that better topical CRS administration can effectively reduce inflammation linked to psoriasis. Ethosomal-mediated skin penetration and sustained drug release work in concert to boost local drug retention within psoriatic lesions while reducing systemic exposure, which is responsible

for the improved therapeutic response. All of these findings show that the optimised ethosomal formulation loaded with CRS is a suitable nanocarrier platform for enhancing topical psoriasis treatment. However, more dermatokinetic, long-term stability, ex vivo skin penetration, and clinical research are needed to validate its translational potential.

7.Conclusion

A QbD-guided ethosomal formulation was effectively created to enhance CRS topical administration. Appropriate vesicle size, low PDI, high drug entrapment, defined shape, and sustained release properties were all incorporated in the optimised formulation. These characteristics imply that ethosomal encapsulation can get around significant drawbacks of applying poorly water-soluble CRS topically. The results offer a solid foundation for the development of CRS-loaded ethosomes for the treatment of psoriasis. Future research should include ex vivo skin penetration and retention, quantitative evaluation of dermal deposition, long-term stability, and suitably planned in vivo pharmacodynamic and safety studies, as the current findings are mainly based on physicochemical and in vitro evaluation. To determine if the noted formulation improvements result in enhanced therapeutic performance in biological systems, such studies will be crucial.

Declaration section

Ethics approval and consent to participate

The experimental protocol received approval from the Institutional Animal Ethics Committee (IAEC) under approval number SDPC/IACE/2025/03. All procedures were carried out in accordance with the guidelines established by the Committee for Control and Supervision of Experiments on Animals (CPCSEA), Government of India, and were consistent with ARRIVE reporting recommendations and OECD guideline 404 for assessment of anti-psoriatic activity.

Declaration of competing interest

The authors declare that they have no known competing financial interests or personal relationships that could have appeared to influence the work reported in this paper.

Data availability

No new data is generated.

Declaration of AI Utilization

AI models such as Grammarly and QuillBot has been used for the refinement of english language in this manuscript.

Funding

None Declared

Clinical trials

Not Applicable

Credit Authorship

Sonam M Gandhi: Data curation, Wrote the manuscript. Methodology, Investigation. **Ronak Dedania:** Conceptualization, Supervision, Project administration and reviewed the manuscript.

References

[1] X. Zhou, Y. Chen, L. Cui, Y. Shi, C. Guo, Advances in the pathogenesis of psoriasis: from keratinocyte perspective, Cell Death Dis 13(1) (2022) 81.
[2] N. Ayala-Fontánez, D.C. Soler, T.S. McCormick, Current knowledge on psoriasis and autoimmune diseases, Psoriasis (Auckl) 6 (2016) 7–32.
[3] G. Girolomoni, R. Strohal, L. Puig, H. Bachelez, J. Barker, W.H. Boehncke, J.C. Prinz, The role of IL-23 and the IL-23/T(H) 17 immune axis in the pathogenesis and treatment of psoriasis, J Eur Acad Dermatol Venereol 31(10) (2017) 1616–1626.
[4] T. Afifi, G. de Gannes, C. Huang, Y. Zhou, Topical therapies for psoriasis: evidence-based review, Can Fam Physician 51(4) (2005) 519–25.
[5] T.C. Ezike, U.S. Okpala, U.L. Onoja, C.P. Nwike, E.C. Ezeako, O.J. Okpara, C.C. Okoroafor, S.C. Eze, O.L. Kalu, E.C. Odoh, U.G. Nwadike, J.O. Ogbodo, B.U. Umeh, E.C. Ossai, B.C. Nwanguma, Advances in drug delivery systems, challenges and future directions, Heliyon 9(6) (2023) e17488.
[6] L. McDowell, B. Olin, Crisaborole: A Novel Nonsteroidal Topical Treatment for Atopic Dermatitis, J Pharm Technol 35(4) (2019) 172–178.
[7] L. Liu, W. Zhao, Q. Ma, Y. Gao, W. Wang, X. Zhang, Y. Dong, T. Zhang, Y. Liang, S. Han, J. Cao, X. Wang, W. Sun, H. Ma, Y. Sun, Functional nano-systems for transdermal drug delivery and skin therapy, Nanoscale Adv 5(6) (2023) 1527–1558.
[8] P. Patra, Cutting-edge advances in transethosomes and nanoethosomes for transdermal drug delivery, Discover Chemistry 2(1) (2025) 148.
[9] D.D. Verma, A. Fahr, Synergistic penetration enhancement effect of ethanol and phospholipids on the topical delivery of cyclosporin A, J Control Release 97(1) (2004) 55–66.
[10] G. Shi, Y. Guo, M. Yang, Development and optimization of a novel nanocarrier SabiWhite-loaded ethosomal gel for targeted skin inflammation complicated by multidrug-resistant pathogens, Front Cell Infect Microbiol 15 (2025) 1640799.
[11] R. Gomathi, A. Bharathiraja, V. Sabitha, K. Snekha, R. Susmitha, P. Gokulram, N. Selvasudha, Vesicular nanocarriers: An innovative targeted and sustained drug delivery system, Next Bioengineering 2 (2026) 100024.

[12] T.O. Ajayi, M.S. Poka, B.A. Witika, Development of bedaquiline nanoemulsions intended for paediatric multidrug-resistant tuberculosis: excipient selection and preformulation studies, Front Med Technol 6 (2024) 1388113.
[13] P. Yadav, B.K. Arjariya, P. Bhawsar, Development and Characterization of Crisaborole-Loaded Liposomal Drug Delivery System for Enhanced Topical and Antibacterial, International Journal of Innovations in Science, Engineering And Management (2026) 61–73.
[14] G. Campillo-Alvarado, T.D. Didden, S.M. Oburn, D.C. Swenson, L.R. MacGillivray, Exploration of Solid Forms of Crisaborole: Crystal Engineering Identifies Polymorphism in Commercial Sources and Facilitates Cocrystal Formation, Crystal Growth & Design 18(8) (2018) 4416–4419.
[15] M. Vivero-Lopez, Design of Polymeric Hydrogels Biomaterials, MDPI-Multidisciplinary Digital Publishing Institute2024.
[16] P. Chaudhari, M. Patani, B. Nangha, H. Sonawane, A. Patel, A. Bokada, S. Upadhyay, Development and Optimization of Crisaborole-Loaded Ethosomes for Enhanced Topical Delivery: Formulation, Characterization and In- Vitro Performance Evaluation, 16 (2026) 261–275.
[17] M.N. Ansari, G.A. Soliman, N.U. Rehman, M.K. Anwer, Crisaborole Loaded Nanoemulsion Based Chitosan Gel: Formulation, Physicochemical Characterization and Wound Healing Studies, Gels 8(5) (2022) 318.
[18] M. Barot, A.P. Prajapati, N. Vadgama, S.B. Narkhede, S. Luhar, Formulation Development and Evaluation of Proniosomal Gel containing Crisaborole, Research Journal of Pharmacy and Technology 18(5) (2025) 2261–2268.
[19] M. Farooq, F. Usman, S. Zaib, H.S. Shah, Q.A. Jamil, F. Akbar Sheikh, A. Khan, S. Rabea, S.A.A. Hagras, G. El-Saber Batiha, I. Khan, Fabrication and Evaluation of Voriconazole Loaded Transethosomal Gel for Enhanced Antifungal and Antileishmanial Activity, Molecules 27(10) (2022).
[20] A. Segall, Preformulation: The Use of FTIR in Compatibility Studies, 4 (2019) 1–06.
[21] M.H. Abdallah, M.M. Shahien, H.E. El-Horany, E.H. Ahmed, Modified Phospholipid Vesicular Gel for Transdermal Drug Delivery: The Influence of Glycerin and/or Ethanol on Their Lipid Bilayer Fluidity and Penetration Characteristics, Gels 11(5) (2025).
[22] L. Gurba-Bryśkiewicz, W. Maruszak, D.A. Smuga, K. Dubiel, M. Wieczorek, Quality by Design (QbD) and Design of Experiments (DOE) as a Strategy for Tuning Lipid Nanoparticle Formulations for RNA Delivery, Biomedicines 11(10) (2023).
[23] Y. Ramaye, M. Dabrio, G. Roebben, V. Kestens, Development and Validation of Optical Methods for Zeta Potential Determination of Silica and Polystyrene Particles in Aqueous Suspensions, Materials (Basel) 14(2) (2021).
[24] E. Touitou, N. Dayan, L. Bergelson, B. Godin, M. Eliaz, Ethosomes - novel vesicular carriers for enhanced delivery: characterization and skin penetration properties, J Control Release 65(3) (2000) 403–18.
[25] E. Wolska, M. Szymańska, Comparison of the In Vitro Drug Release Methods for the Selection of Test Conditions to Characterize Solid Lipid Microparticles, Pharmaceutics 15(2) (2023).
[26] E.-S. Khafagy, B.K. Almutairy, A.S. Abu Lila, Tailoring of novel bile salt stabilized vesicles for enhanced transdermal delivery of simvastatin: a new therapeutic approach against inflammation, Polymers 15(3) (2023) 677.

[27] K. Tang, M. Ao, X. Li, C. Feng, W. Li, Formulation and In Vitro Evaluation of Ethosomal Hydrogel as a Carrier System for Enhancing the Transdermal Delivery of Puerarin, ACS Omega 11(7) (2026) 12214–12228.
[28] Z. Asghar, T. Jamshaid, M. Sajid-Ur-Rehman, U. Jamshaid, H.A. Gad, Novel Transethosomal Gel Containing Miconazole Nitrate; Development, Characterization, and Enhanced Antifungal Activity, Pharmaceutics 15(11) (2023).
[29] S. Chheda, M.M. Rane, Herbal microsponge gel for the treatment of cutaneous lupus erythematosus, Future Journal of Pharmaceutical Sciences 11(1) (2025) 67.
[30] B. Flutter, F.O. Nestle, TLRs to cytokines: mechanistic insights from the imiquimod mouse model of psoriasis, Eur J Immunol 43(12) (2013) 3138–46.
[31] L. van der Fits, S. Mourits, J.S. Voerman, M. Kant, L. Boon, J.D. Laman, F. Cornelissen, A.M. Mus, E. Florencia, E.P. Prens, E. Lubberts, Imiquimod-induced psoriasis-like skin inflammation in mice is mediated via the IL-23/IL-17 axis, J Immunol 182(9) (2009) 5836–45.
[32] C. Weil, R. Adiri, G. Chodick, M. Gersten, E. Cohen Barak, Characteristics of Atopic Dermatitis Patients Treated with Crisaborole: Real-World Data from a Large Healthcare Provider Database in Israel, Clin Cosmet Investig Dermatol 15 (2022) 1205–1211.
[33] P. Chaudhari, M. Patani, B. Nangha, H. Sonawane, A. Patel, A. Bokada, S. Upadhyay, Development and Optimization of Crisaborole-Loaded Ethosomes for Enhanced Topical Delivery: Formulation, Characterization and In-Vitro Performance Evaluation.
[34] I.M. Abdulbaqi, Y. Darwis, N.A. Khan, R.A. Assi, A.A. Khan, Ethosomal nanocarriers: the impact of constituents and formulation techniques on ethosomal properties, in vivo studies, and clinical trials, Int J Nanomedicine 11 (2016) 2279–304.
[35] P. Chouhan, K. Tikariya, U. Atneriya, FORMULATION AND EVALUATION OF 2% CRISABOROLE OINTMENT BY COSOLVENCY METHOD, International Journal of Pharmaceutical Sciences and Medicine 7 (2022) 86–103.
[36] A. Fantini, A. Demurtas, S. Nicoli, C. Padula, S. Pescina, P. Santi, In Vitro Skin Retention of Crisaborole after Topical Application, Pharmaceutics 12(6) (2020).
[37] V. Pacciani, J. Cardellini, A. Balestri, M. Rojas-Rodríguez, M. Calamai, M. Tiboni, L. Casettari, C.E. Saunders, A.A. Karimi, G. Sanità, E. Esposito, A. Zendrini, A. Radeghieri, L. Paolini, P. Bergese, C. Montis, L. Caselli, D. Berti, Ethanol-Guided Hybridization of Extracellular Vesicles with Liquid-Crystalline Lipid Nanoparticles, ACS Appl Mater Interfaces 18(4) (2026) 6530–6548.
[38] E.A. Nieves, M.C. Cotto, F. Márquez, Transferosomes as Drug Delivery Systems: Design Principles, Deformability, and Translational Challenges, Pharmaceuticals 19(6) (2026) 956.
[39] H. Natsheh, E. Touitou, Phospholipid Vesicles for Dermal/Transdermal and Nasal Administration of Active Molecules: The Effect of Surfactants and Alcohols on the Fluidity of Their Lipid Bilayers and Penetration Enhancement Properties, Molecules 25(13) (2020).
[40] Z.A. Nizamudeen, R. Xerri, C. Parmenter, K. Suain, R. Markus, L. Chakrabarti, V. Sottile, Low-Power Sonication Can Alter Extracellular Vesicle Size and Properties, Cells 10(9) (2021).
[41] E. Khodadadi, E. Khodadadi, P. Chaturvedi, M. Moradi, Comprehensive Insights into the Cholesterol-Mediated Modulation of Membrane Function Through Molecular Dynamics Simulations, Membranes (Basel) 15(6) (2025).
[42] R.M. Almuqbil, B. Aldhubiab, Ethosome-Based Transdermal Drug Delivery: Its Structural Components, Preparation Techniques, and Therapeutic Applications Across Metabolic, Chronic, and Oncological Conditions, Pharmaceutics 17(5) (2025).

[43] A.H. Aodah, S. Hashmi, N. Akhtar, Z. Ullah, A. Zafar, R.M. Zaki, S. Khan, M.J. Ansari, T. Jawaid, A. Alam, M.S. Ali, Formulation Development, Optimization by Box-Behnken Design, and In Vitro and Ex Vivo Characterization of Hexatriacontane-Loaded Transethosomal Gel for Antimicrobial Treatment for Skin Infections, Gels 9(4) (2023).
[44] S. Gharat, M. Momin, U. Panchal, A. Omri, Novel ethosomal gel formulation for enhanced transdermal delivery of curcumin and cyclosporine: a preclinical approach to rheumatoid arthritis management, Drug Deliv 32(1) (2025) 2512620.
[45] L. Hua, M. Kaiser, I. Carabadjac, A. Meister, G. Hause, H. Heerklotz, Vesicle budding caused by lysolipid-induced asymmetry stress, Biophys J 122(20) (2023) 4011–4022.
[46] L.A. Kungurova, A.A. Artamonov, E.A. Grigoryev, A.Y. Aronov, O.S. Vezo, R.I. Glushakov, K.A. Kondratov, Morphological Characterization of Plasma-Derived Nanoparticles Isolated by High-Speed Ultracentrifugation: A Scanning Electron Microscopy Study, Int J Mol Sci 26(19) (2025).
[47] P. Colombo, R. Bettini, P. Santi, N. Peppas, Swellable matrices for controlled drug delivery: Gel-layer behaviour, mechanisms and optimal performance, Pharmaceutical Science & Technology Today 3 (2000) 198–204.
[48] W. Zhu, J. Long, M. Shi, Release Kinetics Model Fitting of Drugs with Different Structures from Viscose Fabric, Materials (Basel) 16(8) (2023).
[49] A.A. Mohd Noor, L. Lambuk, F. Ahmad, M. Azlan, N. Mohd Redzwan, Role of dendritic cells and B cells in the skin of imiquimod (IMQ)-induced psoriasis-like mouse model, PeerJ 14 (2026) e20974.
[50] Q. Yan, W. Ye, F. Shan, Y. Shi, Z. Zhang, Z. Cheng, Evaluating the early therapeutic response of radiofrequency ablation in rabbit VX2 lung tumors: a comparison of four diffusion weighted imaging models, Transl Lung Cancer Res 15(4) (2026) 89.
[51] W.R. Swindell, K.A. Michaels, A.J. Sutter, D. Diaconu, Y. Fritz, X. Xing, M.K. Sarkar, Y. Liang, A. Tsoi, J.E. Gudjonsson, N.L. Ward, Imiquimod has strain-dependent effects in mice and does not uniquely model human psoriasis, Genome Med 9(1) (2017) 24.
[52] Y. Cho, J. Kwon, T.S. Kim, Imiquimod promotes Th1 and Th17 responses via NF-κB-driven IL-12 and IL-6 production in an in vitro co-culture model, Exp Ther Med 30(3) (2025) 175.
[53] Y.S. Lee, Preliminary Histological Evidence of Epidermal and DEJ Remodeling with Microneedling-Assisted Topical Exosome Therapy: A Single-Subject Case Report, Clin Cosmet Investig Dermatol 18 (2025) 2377–2385.
[54] Kamini, D. Puri, QbD assisted formulation, optimization and characterization of psoralen phytosome prepared through thin film hydration method, Drug Dev Ind Pharm 52(2) (2026) 291–312.
[55] A. Ababei-Bobu, B. Profire, A.T. Iacob, O.M. Chirliu, F.G. Lupașcu, L. Profire, Niosomes as Vesicular Carriers: From Formulation Strategies to Stimuli-Responsive Innovative Modulations for Targeted Drug Delivery, Pharmaceutics 17(11) (2025).
[56] Sriwidodo, A.K. Umar, N. Wathoni, J.H. Zothantluanga, S. Das, J.A. Luckanagul, Liposome-polymer complex for drug delivery system and vaccine stabilization, Heliyon 8(2) (2022) e08934.
[57] M. Jabeen, A.S. Boisgard, A. Danoy, N. El Kholti, J.P. Salvi, R. Boulieu, B. Fromy, B. Verrier, M. Lamrayah, Advanced Characterization of Imiquimod-Induced Psoriasis-Like Mouse Model, Pharmaceutics 12(9) (2020).